Observations and analysis of sediment diffusivity profiles over sandy rippled beds under waves

Peter D. Thorne[1*], Alan G. Davies[2] and Paul S. Bell[1]

1 Proudman Oceanographic Laboratory, Joseph Proudman Building,
6 Brownlow Street, Liverpool L3 5DA, UK,
Tel 44 (0)151 7954862, Fax 44 (0)151 7954801 pdt@pol.ac.uk,
psb@pol.ac.uk
* corresponding author

2 School of Ocean Sciences, College of Natural Science,
Bangor University, Menai Bridge, Anglesey, LL59 5AB, UK
tel/fax +44 (0) 1248 382884 a.g.davies@bangor.ac.uk

Abstract

Acoustic measurements of near-bed sediment diffusivity profiles are reported. The observations were made over two sandy rippled beds, classified as 'medium' and 'fine' in terms of sand grain size, under slightly asymmetric regular waves. For the medium sand, the ripples that formed had relatively steep slopes, while for the fine sand, the slopes were roughly half that of the medium sand. In the medium sand case, the form of the sediment diffusivity profiles was found to be constant with height above the bed, to a height equal approximately to the equivalent roughness of the bed, k_s, while above this the sediment diffusivity increased linearly with height. For the case of the fine sand there was no constant region; the sediment diffusivity simply increased linearly with height from the bed. To understand the difference between the respective diffusivity profiles, advantage has been taken of the high temporal-spatial resolution available with acoustic systems. Using intra-wave ensemble averaging, detailed images have been built up of the variation in concentration with both the phase of the wave and also height above the bed. These intra-wave observations, combined with measurements of the bed forms and concepts of convective and diffusive entrainment, have been used to elucidate the mixing mechanisms that underlie the form of the diffusivity profiles observed over the two rippled beds. These mechanisms centre on coherent vortex shedding in the case of steeply rippled beds and random turbulent processes above ripples of lower steepness.

I Introduction

In many marine environments, from river estuaries through to the offshore regime, suspended sediments are a significant component of the total sediment transport and, in numerous cases, are dominant. It is therefore necessary to obtain a description of how the sediments are entrained into the water column and to ascertain the resulting form of the suspended sediment concentration profile. Predictions for the form of the concentration profile differ according to the flow, the seabed sediment and, importantly, any resulting bed forms (Sleath, 1984; Soulsby, 1997; Van Rijn et al., 2001). Most of the formulations used have been underpinned by the classical Fickian concept of gradient diffusion (Coleman, 1970; Glenn and Grant, 1987; Vincent and Green, 1990; Vincent and Osborne, 1995; Ogston and Sternberg, 2002; van der Werf et al., 2006), originating from kinetic molecular theory where random molecular movements induce mixing. In the case of suspended sediments in field situations, it is the turbulent fluctuations in the vertical velocity component that give rise to the upward mixing process. In the simplest case the time averaged vertical turbulent diffusive flux of sediment, q_v, is considered to be balanced by the settling of the suspended sediment under gravity, such that:

$$q_v = w_s C \qquad \text{where} \qquad q_v = -\varepsilon_s \frac{\partial C}{\partial z} \tag{1}$$

Here C is the time-averaged sediment concentration at height z above the bed, w_s is the sediment settling velocity, and ε_s is the sediment diffusivity. The vertical profile of ε_s is frequently linked to the eddy viscosity, ν_t, used to model the transfer of momentum by turbulent eddies. The eddy viscosity, ν_t, represents the product of a turbulent velocity scale and a mixing length scale. Both of these factors therefore affect the sediment diffusivity which is commonly expressed as $\varepsilon_s = \beta\nu_t$ where the coefficient β is either assumed to be a constant (equal to unity, or larger or smaller than unity) or is sometimes considered to have a functional dependence upon the sediment in suspension and the flow parameters (Van Rijn, 1984; Whitehouse, 1995; Rose and Thorne, 2001). The vertical profile of ν_t, and hence ε_s, in previous applications has been taken to be constant, linear, parabolic, exponential or some combination thereof (Grant and Madsen, 1979; Nowell and Long, 1983; Nezu and Rodi, 1986; Nielsen, 1992; Van Rijn, 1993; Chung and Van Rijn, 2003). These different forms have been associated with various concepts regarding the mixing in the near-bed boundary layer. Hitherto, there has been no consensus on a general form for profiles of the sediment diffusivity or eddy viscosity, though constant (Nielsen, 1986; van der Werf et al., 2006) and linear profiles (Ribberink and Al-Salem, 1994; Vincent and Osborne, 1995) with height above the bed have been used in many near-bed sediment studies.

Despite the wide use of gradient diffusion, several studies (Sleath, 1982; Hansen et al., 1991; Ribberink and Al-Salem, 1994; Osborne and Vincent, 1992; Fredsøe et al., 1999; Villard and Osborne, 2002; Thorne et al., 2003) have indicated that this is not always the dominant process generating the suspended sediment concentration profile, particularly for sediment entrainment by waves over rippled beds. These studies have shown that, if the ripples are relatively steep with $\eta_r/\lambda_r \geq 0.12$, where η_r is the ripple height and λ_r is the ripple wavelength, then the mixing close to the bed is dominated by a coherent process involving boundary layer separation on the lee-side of the ripple crest during each wave half-cycle near maximum flow velocity. The resulting lee-wake vortex remains attached to the bed entraining sediment into the flow as it grows in size and strength. At flow reversal the sediment-laden vortex is ejected into the water column, carrying sediment to several ripple heights above the bed. This process is coherent and repeatable, with two main periods of sediment entrainment during the cycle at around the times of flow reversal. The sediment mixing process is thus fundamentally different from that associated with gradient diffusion. Gradient diffusion relies on the 'mixing length' being small compared with the vertical extent of the concentration profile as a whole, and the rate of diffusion is proportional to the concentration gradient (Equation (1)). In contrast, the mixing due to vortex entrainment occurs on a (relatively) larger 'convective' length scale that is not, therefore, linked so directly to the concentration gradient. Interestingly, the 'finite mixing length' approach proposed by of Nielsen and Teakle (2004) offers a novel way of reconciling the two different physical concepts contrasted above. Nielsen (1988, 1992) had earlier suggested that in many circumstances, particularly involving rippled beds under waves and also combined waves and currents, both convective and diffusive processes occur together and, in some recent studies (Lee and Hanes, 1996; Lee et al., 2002; Thorne et al., 2002), this approach has been adopted.

The present study represents a contribution towards our understanding of these fundamental mixing processes. Measurements were collected in a large flume, the Deltaflume, Deltares (formerly WL|Delft Hydraulics), the Netherlands, which is 240 m long, 5 m wide and 7 m deep. The size of the flume allowed the wave and sediment transport processes to be studied at full scale (Williams et al., 2003; http://www.wldelft.nl/facil/delta). Simultaneous, closely co-located observations were made of: suspended sediment concentration, suspended particle size, the flow and the ripples on the sandy beds. The data were obtained beneath regular weakly-asymmetrical surface waves over beds of medium and fine sand. These data are used here to examine the sediment diffusivity profiles over the two sandy beds. To interpret the form of the observed sediment diffusivity, advantage is taken of the high temporal-spatial resolution available with acoustic systems. In particular, intra-wave ensemble averaging, coupled with bed form measurements, have been used to build up detailed images of the variation in concentration with both the phase of the wave and also the height above the bed. These data have been used to highlight the underlying entrainment mechanisms that led to the form of the measured sediment diffusivity profiles presented in this study.

The paper is laid out as follows; in Section II a physical discussion is presented of the key modelling concepts, followed in Section III, by a summary of the observational work and data analysis. In Section IV the measurements are presented and interpreted to explain the different profiles for the sediment diffusivity, obtained above the two sandy beds, in terms of convective and diffusive processes. This is followed in Section V by a discussion on the implications of the observations, with conclusions drawn in Section VI.

II Models

A modelling framework can be set out for turbulent oscillatory flows above various naturally occurring bed types in terms of the wave Reynolds number, RE = A_0U_0/ν, where A_0 is the orbital amplitude, U_0 is the near-bed velocity amplitude and ν is the kinematic viscosity, and the relative roughness, A_0/k_s, where k_s is the equivalent bed roughness (Davies and Villaret, 1997). Table 1 summarises a simplified framework for oscillatory flows above erodible sandy beds (see also Davies and Thorne, 2008). Essentially, steeply rippled beds having $\eta_r/\lambda_r \geq 0.12$ occur in low energy flows; such ripples tend to be long-crested (two-dimensional) with vigorous, alternate eddy shedding occurring above them. Such ripples are characterised by low values of RE, A_0/k_s and also of $\hat{\theta} = \hat{\tau}_0 / \{(\rho_s - \rho)gd_{50}\}$ where $\hat{\tau}_0$ is the peak bed shear stress during the wave cycle, ρ_s and ρ are the densities of the sediment and water respectively, and d_{50} is the median grain diameter. For larger values of the respective non-dimensional parameters the ripples are reduced in amplitude and tend to have shorter crest-lengths (2D-3D 'transitional' ripples). Ultimately, for high energy flows, 'dynamically plane' beds occur; here any ripples that are present are of such small steepness ($\eta_r/\lambda_r \leq 0.08$) that the oscillatory flow becomes closely similar *dynamically* to that above a plane bed. [It may be noted that the beds referred to here as 'dynamically plane' are commonly denoted also, in the limit of very high mobility, as 'upper stage plane beds'] The equivalent roughness, k_s, depends upon the grain size for flat sandy beds with, typically, $k_s = 2.5d_{50}$ for 'lower stage plane beds', and upon the ripple height and steepness for rippled beds, $k_s \propto \eta_r(\eta_r/\lambda_r)$, with k_s enhanced by a 'mobile bed' contribution for low ripples and plane beds in high energy flows.

It was noted by Davies and Villaret (1997) that many of the modelling concepts developed for steady turbulent flow remain valid in oscillatory flow. Above smooth flat beds, at high RE, the turbulent eddy viscosity may be assumed to vary linearly with height throughout the wave boundary layer. However, for rougher beds, also at high RE, data suggest the existence of an outer layer in which the turbulent velocity scale decreases with height and in which, therefore, ν_t remains approximately constant (e.g. Trowbridge and Madsen, 1984). The wave boundary layer thickness is overestimated by models that do not include this outer, constant, ν_t-layer. Several eddy viscosity models have assumed, either implicitly or explicitly, that ν_t is also time-varying (Trowbridge and Madsen, 1984; Fredsøe, 1984; Davies, 1986).

The models above are all based upon turbulent diffusion as the dominant mechanism of momentum exchange. In contrast, at lower flow stages above very rough and rippled beds, the situation is entirely different. Here momentum transfer is due mainly to eddy shedding from individual roughness elements at times of flow reversal, and so is well organised in space and time. For relatively low values of RE and A_0/k_s (Table 1) Sleath (1991) and Nielsen (1992) suggested that it is reasonable to treat ν_t as constant in height and time. For the range $1 \leq A_0/k_s \leq 120$, Sleath (1991) proposed the following expression for ν_t by analogy with grid-turbulence experiments:

$$\nu_t = 0.00253 A_0^{3/2} k_s^{1/2} \omega \tag{2}$$

where the angular frequency $\omega = U_0/A_0$. Subsequently, on the basis of data sets for very rough conditions in the range $A_0/k_s < 16$, Nielsen (1992) proposed the constant eddy viscosity:

$$\nu_t = 0.004 A_0 \omega k_s \tag{3}$$

These two formulae give identical results for $A_0/k_s = 2.5$.

Although turbulence is strongly related to eddy shedding, it is the coherent vortex shedding mechanism itself that dominates the mixing in the near-bed layer above very rough and rippled beds. Ranasoma and Sleath (1992) demonstrated experimentally that the effect of turbulent Reynolds stresses above steep ripples is negligible in comparison with the momentum transfer associated with coherent vortices. Their measurements showed large time variations in the vertical transfer of momentum corresponding to the release of coherent vortex structures at the ripple crest. This was reflected in the 'convective eddy viscosity' coefficient used by Davies and Villaret (1997) who introduced time variation into ν_t in order to represent the combined effects on momentum transfer of turbulence and, more importantly, organised eddy shedding at flow reversal.

The vertical mixing of sediment is necessarily closely related to the vertical transfer of momentum. If the bed is flat, the periodic surface-wave-induced vertical velocity, w_w, is very small in the near-bed layer, tending to zero at the bed itself. Thus w_w may be assumed to contribute little to the upward flux of sediment $\overline{w_w C_w}$ near the bed, where C_w is the periodic component of the suspended concentration and the over-bar denotes time averaging. Rather higher above the bed, it has been shown by Sheng and Hay (1995) that this flux remains relatively small, with typically $\left|\overline{w_w C_w} / w_s C\right| < 0.2$. This suggests the validity of the following approximation, related to turbulent processes only, for the upward sediment flux above a flat bed (c.f. Equation (1)):

$$-\overline{C'w'} \approx \varepsilon_s \frac{dC}{dz} \tag{4}$$

where the primes here denote, respectively, the random turbulent contributions to the concentration and the vertical velocity.

In contrast, above a rippled bed, the sloping sides of the bed forms give rise to locally significant, periodic, vertical velocity contributions arising from both the (frictionless) wave action and the (frictional) process of vortex formation. Thus, in a ripple-averaged sense, the (convective) term $\overline{w_w C_w}$ can contribute significantly to the upward flux of sediment; in fact, this term can dominate the upward sediment flux in the bottom part of the wave boundary layer.

If the sediment diffusivity ε_s is still identified solely with the turbulent flux $\overline{C'w'}$ (c.f. Equation (4)), then the time-averaged sediment balance in the case of a rippled bed may be expressed:

$$-w_s C + \overline{w_w C_w} - \varepsilon_s \frac{dC}{dz} = 0 \tag{5}$$

such that

$$\varepsilon_s = \frac{-w_s C + \overline{w_w C_w}}{dC/dz} \tag{6}$$

In the present paper, however, we effectively absorb the convective transfer represented by $\overline{w_w C_w}$ into a ‘convective diffusivity’ whereby ε_s is defined simply by

$$\varepsilon_s = \frac{-w_s C}{dC/dz} \tag{7}$$

The physically interesting and practically significant consequences of this widely used technique are discussed in Section IV where we obtain contrasting vertical profiles for ε_s based on observations made in the Deltaflume above beds of different grain size. These measured ε_s profiles are compared with three established expressions for ε_s; two of these were specifically formulated for waves propagating above rippled and very rough sand beds, while the third, a linearly increasing diffusivity, is that most commonly used in sediment and flow studies involving plane beds (Grant and Madsen, 1979; Lee and Hanes, 1996; Lee, Friedrichs and Vincent, 2002). These expressions are discussed here in turn.

Firstly, Nielsen's (1992) sediment diffusivity for rough and rippled beds follows from the eddy viscosity formulation (3) and the relationship $\varepsilon_s = \beta\nu_t$ wherein the value adopted for β reflects the relatively high efficiency of the eddy shedding process in entraining sediment into suspension. In particular, Nielsen (1992) adopted $\beta = 4$ leading to the following expression for the near-bed sediment diffusivity:

$$\varepsilon_s = 0.016\, k_s U_o \tag{8}$$

The physical explanation for the large value of β used by Nielsen and others has not been fully explained by either models or experiments. However, it would appear to be linked to 2D and/or 3D temporal-spatial correlations between the instantaneous velocity and concentration fields, as shown by Magar and Davies (2005) using a particle tracking model.

Nielsen's (1992) proposed expression for the equivalent roughness k_s in equation (8) was $k_s = \delta\eta_r(\eta_r/\lambda_r)$ where $\delta = 8$. However, as explored by Thorne et al. (2002), this rather low value for δ does not take into account the convective contribution to the upward mixing of momentum and sediment. Here therefore, following Thorne et al. (2002) we have adopted the more commonly used value $\delta = 25$ (Swart, 1974) in equation (8) and determined ε_s using detailed in-situ measurements of the ripple dimensions, η_r and λ_r, made in the Deltaflume.

The second formulation for ε_s highlighted in Section IV is that of Van Rijn (1993). This was derived empirically for waves alone and involves a three-layer structure for

ε_s covering the full water column. Importantly, it represents the sediment diffusivity in the near-bed layer ($z \le \zeta_s$) as being constant with height:

$$\varepsilon_s = \varepsilon_b \qquad z \le \zeta_s \qquad 9(a)$$

$$\varepsilon_s = \varepsilon_m \qquad z \ge 0.5h \qquad 9(b)$$

$$\varepsilon_s = \varepsilon_b + (\varepsilon_m - \varepsilon_b)\left[\frac{z-\zeta_s}{0.5h-\zeta_s}\right] \qquad \zeta_s < z < 0.5h \qquad 9(c)$$

Here ε_b and ε_m are, respectively, constant values for the sediment diffusivity near the bed and in the upper half of the water column, with the latter value being the larger; ζ_s is the thickness of the near-bed mixing layer and h is the water depth. This eddy diffusivity is constant in the near-bed layer, is linearly increasing with height in the layer above this, and then remains constant in the upper half of the flow. Van Rijn suggested a lower layer thickness given by $\zeta_s = 3\eta_r$. In the present paper, we have adopted the expression $\zeta_s = k_s$ ($=25\eta_r(\eta_r/\lambda_r)$) for ease of comparison with Nielsen's formulation. It may be noted that Van Rijn's expression is recovered from this for ripples having a steepness of $\eta_r/\lambda_r = 0.12$. In Section IV, due to variations in the observed ripple steepness in different experimental runs, this results in $\zeta_s = (3.4\pm0.2)\eta_r$ for the medium sand bed and $\zeta_s \approx (1.9\pm0.2)\eta_r$ for the fine sand bed. Assuming that $\zeta_s = k_s$, Van Rijn's formulation can be expressed in the same form as that of Nielsen, namely:

$$\varepsilon_b = \alpha_b k_s U_o \qquad (10)$$

in which Van Rijn's coefficient $\alpha_b = 0.004D_*$, wherein the dimensionless grain size $D_* = d_{50}[(s-1)g/\upsilon^2]^{1/3}$; s is the relative density ρ_s/ρ, ρ_s is the grain density and ρ is the fluid density; g is the acceleration due to gravity; and υ is the kinematic viscosity. The eddy diffusivity in the upper layer is given by Van Rijn (1993) as:

$$\varepsilon_m = \alpha_m \frac{Hh}{T} \qquad (11)$$

where H is the wave height, T is the wave period and the empirical coefficient α_m=0.035. In the present study, where the measurements were confined to the bottom quarter of the water column, it is only predictions for the near-bed constant and linear regions that are assessed.

The final form used for the sediment diffusivity is a simple linear increase in ε_s with height above the bed. This is commonly expressed (Grant and Madsen, 1979; Lee and Hanes, 1996; Lee, Friedrichs and Vincent, 2002) as

$$\varepsilon_s = \beta\kappa\bar{u}_* z \tag{12}$$

where κ=0.4 is Von Karman's constant. Here we have used the mean magnitude of the friction velocity, $\bar{u}_*$, in the wave cycle as representative of the turbulent mixing during the wave cycle as a whole (see Davies, 1986):

$$\bar{u}_* = 0.763(f_w/2)^{0.5}U_o \quad \text{and} \qquad f_w = 0.237\left(\frac{k_s}{A_o}\right)^{0.52} \tag{13}$$

where f_w is the friction factor formulated by Soulsby (1997). In applying equation (12) to the observations, consideration must be given to the appropriate expression to be used for k_s in the analysis. For a flat (or lower stage plane) bed the Nikuradse roughness value is normally used which, as noted earlier, is commonly expressed as k_s=2.5d_{50}. The implications of using this skin-friction expression over a rippled bed are considered in Section IV.

III Experimental arrangement and data analysis

The study was undertaken as part of a collaborative European experiment, and was conducted in the Deltaflume. Details of the experimental arrangement have been provided in an earlier publication (Thorne et al., 2002) and are therefore only briefly summarised here for completeness. The large size of this flume, 240 m in length, 5 m in width and 7 m deep, allow hydrodynamic and sediment transport phenomena to be studied at full scale. The experiments were conducted beneath weakly-asymmetrical, regular, surface waves with heights, H, and periods, T, in the respective ranges H=0.6-1.1 m and T=4–6 s for the medium sand and H=0.5-1.1 m and T=4–5 s for the fine sand. Therefore the hydrodynamic conditions for the experiments involving the two sands were comparable. The medium sand had d_{10}=170 μm, d_{50}=330 μm and d_{90}=700 μm, while the fine sand had d_{10}=95 μm, d_{50}=160 μm and d_{90}=300 μm; both the sands were therefore reasonably well sorted. The sediments were located in a layer of thickness 0.5 m and length 30 m, approximately halfway along the flume, where the mean water depth was 4.5 m. The measurements were conducted first above the medium sand bed; this was then removed and replaced by the fine sand bed.

Figure 1 shows the instrumented tripod platform 'STABLE' (Sediment Transport And Boundary Layer Equipment) used to collect the measurements. The main instruments on STABLE relevant to the present study were: a multi-frequency acoustic backscatter system, ABS, a pumped sampling system, an acoustic ripple profiler, ARP, and electromagnetic current meters, ECMs. All measurements were synchronised. A study of the impact of STABLE on the processes being measured was shown to be minimal (Williams et al., 2003). Typically an experiment consisted of propagating waves over the bed for about an hour, until the bed-forms came to nominal equilibrium, and then collecting data for a 17 min period.

High-resolution vertical profiles of the suspended sediments were measured using a triple-frequency ABS (Crawford and Hay, 1993; Thorne et al., 1997; Thorne and Hanes, 2002). The ABS provided 128 backscatter profiles each second, at each of the three frequencies, 1 MHz, 2 MHz and 4 MHz. Each profile consisted of 128 range bins, with a spatial resolution of 0.01 m, thereby covering a range of 1.28 m. Physical samples of the suspension were obtained by pumping through nozzles (Bosman et al., 1987) located at ten heights above the bed between 0.053-1.55 m. The collected samples of the suspension were sieved to provide the mass size distribution with height above the bed. They were used to calibrate and assess the veracity of the acoustic backscatter measurements and provide profiles of w_s. To establish whether ripples were present on the bed, and to monitor their evolution and migration, a specifically designed acoustic ripple profiler, ARP, (Bell et al., 1998; Thorne et al., 2002; Williams et al, 2004) was used. The ARP operated at 2.0 MHz, and provided sub-centimetric measurements of the bed location over a 3m transect along the direction of wave propagation. To measure the flow three ECMs were located at 0.3, 0.6 and 0.91 m above the bed. They provided measurements of the along-flume and vertical components of the flow velocity at 8 Hz.

Measurements of the suspended concentration were collected with the ABS. Using the particle size data obtained from the pumped samples an explicit acoustic inversion (Thorne and Hanes, 2002) was carried out on the recorded 17 min averaged backscatter voltages to convert them to mean concentration profiles. For each experiment three independent concentration profiles were obtained, one for each frequency. Since 13 experiments were carried out above the medium sand and 7 were carried out above the fine sand, this resulted in 39 and 21 mean concentration profiles in the respective cases. Using the bed echoes the concentration profiles were referenced to the undisturbed bed, such that in the plots that follow z is the height above the undisturbed bed, with a vertical sampling interval of 0.01 m. The veracity of the profiles has been assessed previously (Thorne et al., 2002) using the pumped sample measurements and this is not repeated here. However, for the purpose of illustrating the magnitude and form of the concentration profiles for the two sands, examples are provided in Figure 2 for wave conditions H=0.5 m and 0.8 m and T=5 s. The figure shows mean concentrations, averaged over the burst period (17 min, ~200 wave cycles), at the three acoustic frequencies for the two sands. The detailed differences between the profiles at the three frequencies are due the accuracy of the system calibration, the model used for the acoustic scattering properties of the suspended sediments and the inversion methodology employed. However, the important factor as far as this study is concerned is that the general profile features are consistent across the three frequencies. For the H=0.5 m case it can be seen that the magnitude of the suspended concentration for the fine sand (x,*,Δ) is significantly greater than for the medium sand (+,o,□). This was also the case for H=0.8 m, though the difference was less. This was a general trend for the two sands, with the difference in suspended concentration levels decreasing as wave height increased. The form of the profiles can also be seen to be different, with the relative reduction in concentration being greater for the fine sand in the first 0.1 m above the bed while, between 0.1-0.4 m, the medium sand concentration reduces somewhat more rapidly than the fine. Above 0.4 m the gradients become comparable for the two sands.

Using the mean concentration profiles, the sediment diffusivities ε_s were calculated for each experiment using equation (7), with w_s determined from a d_{50s} particle size profile empirically fitted to the pumped sample data. The expressions used were:

$$\varepsilon_s = \frac{-\dfrac{w_{sj}+w_{sk}}{2}\dfrac{C_j+C_k}{2}}{\dfrac{(C_k-C_j)}{\Delta_{jk}}} \tag{14a}$$

$$z = \frac{z_j+z_k}{2} \tag{14b}$$

with w_s given by Soulsby (1997) as:

$$w_s = \frac{\nu}{d_{50s}}[(10.36^2+1.049D_*^{\ 3})^{0.5}-10.36] \tag{14c}$$

where Δ_{jk} was the separation between range bins j and k. For the near-bed layer 0.01-0.21 m above the bed, j and k were taken as adjacent range bins while, between 0.21-0.43 m, j and k were defined as two range bins apart and, above 0.43 m, as four range bins apart. This increase in the separation of j and k with height above the bed smoothed the derivative of the concentration profile and reduced scatter in the diffusivity profiles.

The resulting sediment diffusivity profiles were next normalised using four different non-dimensional scalings and they were also averaged in three different ways. The aim here was to clarify the trends in ε_s and assess whether the different approaches gave consistent results. The four normalisations used for height z and sediment diffusivity ε_s were, respectively:

$$z/h \qquad \varepsilon_s/\kappa\bar{u}_* h \tag{15a}$$

$$z/\delta_w \qquad \varepsilon_s/\kappa\bar{u}_*\delta_w \tag{15b}$$

$$z/\eta_r \qquad \varepsilon_s/U_o\eta_r \tag{15c}$$

$$z/k_s \qquad \varepsilon_s/U_o k_s \tag{15d}$$

The first two of the normalisations have been used by previous authors (eg Sheng and Hay, 1995) and the latter two were chosen here on the basis of the theoretical expressions in section II. The scale thickness of the wave boundary layer δ_w has been taken here as:

$$\delta_w = \bar{u}_*/\omega = 0.763(f_w/2)^{0.5}U_o/\omega, \tag{16}$$

For the normalisations in equations (15b) and (15d), the equivalent bed roughness has been taken as $k_s=25\eta_r(\eta_r/\lambda_r)$. The three averages used on the normalized ε_s data at each range bin above the bed were (i) the median which is a relatively robust mean with regard to outliers; (ii) a trimmed mean value which excluded the 20% highest and 20% lowest data values; and (iii) a mean based on a simple in-house filter that rejected outliers. These normalised averages were then smoothed using localised vertical averaging over intervals that increased in extent with height above the bed, in order to further reduce the scatter in the resulting ε_s profiles. Range bins 1-20 above the bed had no averaging applied; range bins 21-40 were averaged over three adjacent bins; and bins 41-86 were averaged over five adjacent bins.

IV Sediment diffusivity measurements and interpretation

(i) Medium sand

Using equation (14), ε_s was calculated above the medium sand bed using the ABS concentration profiles, together with the pumped sample particle size profiles. The values for the suspended sediment size varied from around d_{50s}=230 μm within a centimetre or two of the bed, to about d_{50s}=170 μm at 1 m above the bed. The reduction in particle size, of about a 30% in the bottom metre above the bed, is small compared with the change in concentration and had a second order effect on the variation of ε_s with height above the bed. The results for the 39 sediment diffusivity profiles, from the 13 experiments involving the medium sand, are shown in Figure 3. Here it can be seen that the sediment diffusivity is relatively consistent in form in the bottom 0.2 m above the bed, having values around 0.001-0.003 m^2s^{-1}. Above 0.2 m the values for the sediment diffusivity increase with height above the bed and the scatter in the data increases. This increase in scatter with height is due both to noisier lower concentration levels at the greater heights and also to the different flow and bed conditions associated with the thirteen different experiments. In an attempt to clarify trends in the data, the normalisations in equation (15) were applied to the respective sediment diffusivity profiles. The normalized data, shown by the small solid dots in Figure 4, have a scatter which is approximately one third that of the data shown in figure 3 and an enhancement in the form of the trends. Although none of the four normalizations collapse all the data on to a single profile, they clearly show a common trend in the sediment diffusivity profile, with a near-bed region that is nominally constant with height above the bed, above which there is a trend of increasing diffusivity with height. It can also be seen that the four different normalizations yield comparable clustering of the data. These normalised data were next averaged and smoothed using the three approaches described at the end of section III. This gave the three averaged results shown in Figures 4(a) to (d), respectively. These averaged profiles clarify significantly the form of the normalized sediment diffusivity with height above the bed. Also, since the different averaging schemes give very comparable results, the veracity of the final trends in the normalised sediment diffusivity profile is considered to be high.

The final result, obtained using the normalization given by equation (15d), together with averaging over the three means, is the profile shown in Figure 5 represented by the large solid circles. The error bars shown on the final ε_s profile were not derived from the three averages, but were calculated from the whole data set, shown by the small solid dots in Figure 4, at each height above the bed. The data show approximately constant normalised sediment diffusivity in the region below $z/k_s \approx 1.3$. At heights greater than $z/k_s \approx 1.3$, $\varepsilon_s/U_o k_s$ increases linearly, though above about $z/k_s > 3$, the trend in the data becomes less clear due to increasing scatter, mainly arising from taking the derivative of rather noisy low concentration data at these greater heights above the bed. However, notwithstanding this increase in scatter with height, the data clearly show a normalised sediment diffusivity that is approximately constant for $z/k_s \leq 1.3$ and above which there is a linear increase with height.

Using equation (8), Nielsen's empirical prediction for the constant normalized sediment diffusivity was calculated. This is shown by the dotted line in Figure 5 and has a value of 0.016. This prediction is somewhat less than the presently inferred, measured value of 0.029. The lower value given by equation (8) could indicate that Nielsen's assumed value of $\beta = 4$ linking the sediment diffusivity to the eddy viscosity should be larger, or that the constant term of 0.004 in equation (3) is somewhat underestimated. In any event, the agreement between Nielsen's predictions and the measurements is not considered to be unreasonable, given the accuracy of the previously available data upon which equation (8) was based.

Considering next the Van Rijn formulation for the constant sediment diffusivity layer, the value predicted by equations (9a & 10) is 0.028 which is very close to the value obtained here. Given the limited measurements upon which equations (9a & 10) were based, the agreement may be somewhat fortuitous. However, the main feature of a near bed constant diffusivity, with a value close to both Nielsen's and Van Rijn's predictions, does indicate that the present observed magnitude and form for the sediment diffusivity is not unreasonable. Unlike the Nielsen formulation, the Van Rijn one also involves a linearly increasing sediment diffusivity above $z/k_s > 1$. Using equation (9b, 9c & 11) the predicted linear portion of the normalized sediment diffusivity does not result in a single curve for the present normalization. Therefore, rather than showing the calculations for each case, the bounds from the calculations are given by the two dashed lines. The spread is not large and is associated primarily with changes in the wave period, together with the assumptions implicit in the determination of ε_m via Equations (9b) and (11) which cannot be validated here. Again, given the limited data upon which equations (9-11) were based, the predictions are considered to be in reasonable agreement with the present data, though overestimating their value in the linear region. However, simply by increasing the lower layer thickness ζ_s from k_s to $1.3k_s$ brings the centre line of the linear predictions much closer to the observations.

To complete the comparison of predictions with observations, equation (12) has been evaluated using equation (13), and the result has then been normalised to yield:

$$\frac{\varepsilon_s}{k_s U_o} = 0.763\kappa\beta\sqrt{\frac{f_w}{2}}\frac{z}{k_s} \qquad (17)$$

If equation (17) is evaluated using a mean value for f_w, from all the medium sand experiments, calculated using $k_s=25\eta_r(\eta_r/\lambda_r)$ in equation (13) and with $\beta=1$, the predictions for the sediment diffusivity ('×' in Figure 5) substantially overestimate the observed values in the linear region. However, if f_w is calculated using a flat bed approximation $k_s=2.5d_{50}$ based on the grain size, then equation (17), again with $\beta=1$, yields the line in Figure 5 represented by the '+' symbols. Evidently this latter outcome compares very favourably with the data in the linear region, with only a marginal underestimation of the diffusivity occurring. However, this result could be coincidental, since, from equations (12) and (13), $\overline{u}_*$ has only a weak power dependence upon k_s of 0.26. In any event, what is clear is that the use of equation (12), with an equivalent roughness based on $k_s=25\eta_r(\eta_r/\lambda_r)$, significantly overestimates the present observations of sediment diffusivity.

Finally, in order to capture the behaviour of the diffusivity in this case involving the medium sand, simple expressions have been fitted to the present data set to yield empirical expressions for the variation of sediment diffusivity with height above the bed. These expressions, which are consistent with those of both Nielsen and Van Rijn in the bottom layer and with Van Rijn in the linear layer above this, are as follows:

$$\varepsilon_s = \xi_1 U_o k_s \qquad z \leq 1.3 k_s \qquad (18a)$$

$$\varepsilon_s = \xi_2 U_o z - \xi_3 U_o k_s \qquad z \geq 1.3 k_s \qquad (18b)$$

where ξ_1=0.029, ξ_2=0.028, ξ_3=0.007 and the expression is given by the solid line in figure 5. Although it is acknowledged that the parameter space of the present study is relatively limited, it was considered of interest to put the above expressions forward, since they are compatible with the other formulations and suitable for comparison with diffusivities based on any new or emerging data sets.

To elucidate the processes underlying the form of the sediment diffusivity profile, both the bed forms and also the variation of suspended sediment concentration with the phase of the wave and height above the bed were examined. This takes advantage of the bed form measuring capability of acoustics and the high spatial and temporal resolution of suspension measurements also provided by acoustics. To illustrate the type of bed forms present on the medium sand, a typical measurement from the ARP is shown in Figure 6a. The plot shows the development of a transect, over a 17 min period, for the case of T=5 s and H=0.81 m. The ripples were well developed with mean dimensions of λ_r=0.34 m, η_r=0.047 m, and therefore slope of η_r/λ_r=0.14. This was typical for the medium sand, with η_r and λ_r lying respectively in the range 0.04 – 0.06 m and 0.26 – 0.51 m and with η_r/λ_r= 0.12-0.15. Plots of the ripple slopes and equivalent roughness, given by $k_s=25\eta_r(\eta_r/\lambda_r)$, are shown in Figures 6b and 6c. The ripple slopes had a mean value of 0.14 which implies that vortex formation and entrainment should have occurred (Sleath, 1984). Also the roughness of the bed is quite large, around 0.17 m, indicating that the bed is having a major impact on the near-bed flow.

To assess the mechanisms of sediment entrainment directly over the medium sand, intra-wave processes were investigated. The results are shown in Figure 7; here the intra-wave height variation of the ripple-averaged suspended sediment concentration, has been constructed using ensemble wave phase-averaging with an 18° interval over

200 wave cycles as the ripple slowly migrated below the ABS over the 17 min recording period. The wave conditions were H=1.06 m and T=5s. It can be seen clearly that there are two main entrainment events and that these occur close to flow reversal; they do not coincide with maximum flow. Further analysis of this data (Thorne et al., 2003; Davies and Thorne, 2005) supported the concept that the observations shown in Figure 7 can be interpreted as arising from flow separation on the lee slope of the ripple, with the consequent generation of growing lee slope vortices (Sleath, 1982; Hansen et al., 1991; Vincent et al., 1999; van der Werf et al. 2007). The vortices, while attached to the bed, entrain sediment and become sediment laden. Then, near flow reversal, they are lifted up into the water column, carrying sediment away from the bed. The processes are not random, but are repeatable and coherent. Importantly, the layer in which these effects occur may be seen to correspond to several ripple heights in thickness.

The intra-wave observations in Figure 7 may be related to the sediment diffusivity profile in Figure 5 in the following way. Due to the formation of vortices on the ripple lee slopes, suspended sediments were contained within a relatively fixed mixing region, of height comparable with the ripple height η_r, for most of the wave cycle. Near flow reversal the vortices were lifted up into the water column, retaining their structure to a height of the order of k_s. This is consistent with the detailed flow measurements made by Ranasoma and Sleath (1992) who concluded that vortex shedding effects dominate the dynamics in a near-bed layer of thickness at least one or two ripple heights above the ripple crest level. It is the associated coherence of sediment entrainment and structure that leads to the constant value for the sediment diffusivity within about $z/k_s \leq 1.3$ ($3\eta_r$-$4\eta_r$ for the medium sand). At heights greater than $z/k_s \approx 1.3$, the coherent structure of the vortices breaks down, with mixing of momentum increasingly becoming dominated by random turbulent processes (Ranasoma and Sleath, 1992). Here, therefore, gradient diffusion dominates and mixing increases due to an increase in the mixing length scale with height above the bed, leading to the linear increase in sediment diffusivity above the vortex layer.

(ii) Fine sand

Again using equation (14), ε_s was calculated for the fine sand bed, using the ABS concentration profiles together with the pumped sample particle size profiles. The values for the suspended sediment size in this case varied from around d_{50s}=125 μm within a centimetre or two of the bed, to about d_{50s}=90 μm at 1 m above the bed. As with the medium sand the change in particle size with height above the bed did not strongly affect the form of the diffusivity profile. The results for the 21 sediment diffusivity profiles, from the 7 experiments involving the fine sand, are shown in Figure 8. Unlike the results for the medium sand, there does not appear to be a region of constant sediment diffusivity just above the bed. In contrast, the sediment diffusivity can be seen to increase from around 0.0002-0.0006 m^2s^{-1} close to the bed, to values in the region of 0.003-0.01 m^2s^{-1} at 0.8 m above the bed. These values for ε_s are around one fifth of those for the medium sand near the bed, but are more comparable in magnitude at about 0.8 m above the bed. As with the medium sand, the scatter in the data increases with height above the bed, due to noisier lower concentration levels at greater heights and due also to the different flow and bed conditions associated with the different experiments. Following the same methodology as described earlier, four normalisations and three averaging procedures were applied to the sediment diffusivity profiles. The results are shown in Figure 9. The different normalisations and averages give consistent results, particularly in Figures 9b-9d which show no indication of a constant diffusivity near-bed layer, but instead exhibit a sediment diffusivity that increases linearly with height above the bed. As with the medium sand, the final normalisation, namely equation 15(d), with a mean taken from the three averaging schemes, was used to produce the final result shown in Figure 10. This shows no indication of a near-bed constant sediment diffusivity, associated in the medium sand measurements with vortex formation and entrainment of sediments. Instead, the results show, in the near-bed region, that the normalised sediment diffusivity increases linearly with height above the bed. Because there is no obvious constant near-bed sediment diffusivity, no useful comparison can be made with the formulations of Nielsen (Eq. (8)) or Van Rijn (Eq. (10)). However, it is possible to compare Van Rijn's linearly increasing sediment diffusivity region with the present data. If, in equation (9c), ζ_s and ε_b are set to zero, then using linear wave theory in the determination of ε_m we have

$$\frac{\varepsilon_s}{k_s U_o} = \frac{2\alpha_m}{\pi}\sinh(kh)\frac{z}{k_s} \qquad (19)$$

where k is the wave number of the surface waves. Using this expression and taking the mean value of k for all the fine sand experiments, the dashed line in Figure 10 is obtained. Evidently the resulting, predicted, normalised sediment diffusivity is comparable with the observed values, though it somewhat overestimates them. Reducing α_m from 0.035 to 0.022 brings Van Rijn's expression into line with the observations. Given the limited data set upon which equation (9c) is based, this adjustment does not seem unreasonable. Secondly, equation (12) expressed in the form of equation (17) was compared with the data. It is interesting to note that, if equation (17) is evaluated using $k_s=25\eta_r(\eta_r/\lambda_r)$ in equation (12), with $\beta=1$, as shown by the '×' symbols in Figure 10 the predictions again significantly overestimate the observed values. However, if the flat bed approximation $k_s=2.5d_{50}$ is used, the line in Figure 10 represented by the '+' symbol is obtained, which can be seen to compare favourably with the data, with only a minor overestimation occurring. Given both these fine sand results and also those for the medium sand, it does appear to be the case that the use of $k_s=25\eta_r(\eta_r/\lambda_r)$, for a rippled bed, overestimates the roughness length substantially if equation (12) is used to calculate ε_s.

Finally if, as in the medium sand case, an empirical fit is made to the data, forcing $\varepsilon_s=0$ at z=0, then the following expression results:

$$\varepsilon_s = \chi_1 U_o z \qquad (20)$$

where $\chi_1=0.017$. This is comparable, though a somewhat smaller gradient than that for the linearly increasing region of the sediment diffusivity in the medium sand case.

To explain the form of the sediment diffusivity over the fine sand and its difference from the medium sand, we have again looked at the bed forms. Figure 11 shows a typical example of the bed-forms, with associated plots of the ripple slopes and the equivalent bed roughness. Figure 11a shows the ripple formation for waves with T=5 s and H=0.79 m; these inputs are very comparable with the case shown in Figure 6a for the medium sand. However, for the fine sand the ripples can be seen to be less well developed and less coherent in form, with, in the case shown, η_r=0.019 m, λ_r=0.27 m and η_r/λ_r=0.07. This was typical of all the experiments, with η_r and λ_r respectively being in the ranges 0.01 – 0.03 m and 0.15 – 0.84 m and, as shown in Figure 11b, with η_r/λ_r= 0.06-0.09. For this range of slopes no significant flow separation or vortex formation is expected to occur (e.g. Sleath 1984). Therefore, although the ripples enhanced the bed roughness somewhat, they acted on the flow dynamically like a plane bed. As seen in Figure 11c, the equivalent roughness of the bed, if based upon $k_s=25\eta_r(\eta_r/\lambda_r)$, would be just over a quarter that of that in the medium sand case, indicating that the impact of the bed on the flow is restricted to a region much closer to the bed than for the medium sand. However, the roughness of a dynamically plane bed is more appropriately defined simply in terms of the sediment grain size, as discussed earlier with reference to Figure 10.

To assess the impact of ripples of low slope on sediment entrainment, the variation of the suspended sediment with the phase of the wave and the height above the bed of fine sand was examined. As in the case of the medium sand, the result was constructed using ensemble wave phase averaging over 200 wave cycles. An example of the results is shown in Figure 12 for the following wave conditions: H=0.82 m and T=5s. The structure of the intra-wave suspended sediments is seen to be quite different from that shown in Figure 7; there are no significant suspension events near flow reversal lifting sediment well up into the water column. High concentrations are confined to a relatively thin layer within a few centimetres of the bed and the variation in the suspended load seems to be only weakly dependent on the phase of the wave, with only marginal increases in suspended concentration levels at maximum flow speed. The results in Figure 12 indicate that the bed is behaving dynamically more like a plane bed, rather than a bed that is inducing vortex formation and entrainment. Therefore, the lack of a constant sediment diffusivity region in the fine sand case is not surprising, since the conditions for vortex entrainment were not present and it is the formation of vortices which are considered to be the underlying process leading to the constant sediment diffusivity region. For the fine sand case it is considered that the dynamics are comparable with the classical flat bed situation and that turbulent processes dominate the near-bed sediment entrainment. In this case the turbulent eddies are considered to grow with height above the bed (Davies and Villaret, 1997), leading to the linear increase in sediment diffusivity measured in this study over the bottom quarter of the water column.

V Discussion

The aim of the present study was to contribute to the detailed understanding of the form of the sediment diffusivity profile above a rippled bed and elucidate the underlying mechanisms that give rise to the ε_s-profile. This was stimulated by the contrasting descriptions of sediment entrainment due to the processes of gradient diffusion and vortex shedding, the former being associated with random turbulence and the latter with repeatable coherent structures. The gradient diffusion process, where the 'mixing length' is considered small compared with the vertical extent of the concentration profile, is readily represented via the concept of a sediment diffusivity; in contrast, the vortex shedding process cannot be so directly associated conceptually with a diffusion rate dependent upon the concentration gradient. The present work was aimed at examining the relationship between the different processes and their widely used representation via the formulation of a sediment diffusivity profile.

The occurrence of vortex shedding in the oscillatory boundary layer above ripples depends upon the ripple steepness and, more subtly, on the detailed shape of the ripple crests. Roughly speaking, vortex shedding is expected to occur if η_r/λ_r is greater than about 0.12 and 'dynamically plane' bed conditions are expected if the steepness is less than about 0.08. In the Deltaflume experiments reported here, the ripple steepness above the medium and fine sands was consistently close to 0.14 and 0.07, respectively, suggesting that in the medium sand case vortex shedding was occurring while in the fine sand case it was not. This proposition was confirmed by the intra-wave observations described in the previous section, and was translated into the contrasting forms found for the respective diffusivity profiles, namely 'constant + linear' for the medium sand and 'linear' for the fine sand. The reason why ripples of different steepness were generated by essentially the same wave conditions is beyond the scope of the present paper. The difference between the medium and fine sand sizes may have given rise, for example, to some different combination of bed load and suspended load processes that promoted ripple development in the medium sand case and inhibited it in the fine sand case. Probably, in the latter case, the relatively larger amount of suspended sediment gave rise to settling patterns over the ripple surface that counteracted any tendency for the ripples to grow (see O'Donoghue et al 2006 for more detailed discussions). In any event, the two sand sizes highlighted in this paper exemplified very clearly the consequences of the ripple steepness for the mixing processes in the wave boundary layer, which form a key part of the complex 'triad of interactions' between the oscillating flow, the bed forms and the sediment transport processes.

With regard to the modelling framework introduced in Section II and Table 1, it is interesting to note that the experiments conducted here had Reynolds numbers in the same approximate range; RE ~ $3.2.10^4$-$2.1.10^5$ for the medium sand $2.8.10^4$ - $1.4.10^5$ for the fine sand. However the relative roughness, A_0/k_s, in the medium and fine sand cases was significantly different. In the medium sand case, with $k_s=25\eta_r(\eta_r/\lambda_r)$, A_0/k_s lay in the range 1.3-3.1, while for the fine sand, with $k_s=2.5d_{50}$, A_0/k_s lay in the range 470 -1060. The expected 'bed form characteristics' in Table 1 are necessarily well matched with the respective A_0/k_s values in the experiments, by the above choice of dynamically based roughness. However Table 1 implies a rather oversimplified link between A_0/k_s and RE, which is not borne out by the present observations, ie RE values were comparable, while k_s differed by more than two orders of magnitude. As explained by Davies and Villaret (1997) the two parameters need to be treated as independent of one another, in a way that depends in practice on the triad of interactions referred to above.

The relevance of achieving greater understanding of the sediment diffusivity above bed forms is considerable. The prediction of the bed roughness still remains a central obstacle in the accurate prediction of sand transport rates. As illustrated in the present study, misinterpretation of the type of flow and/or misuse of the bed roughness k_s can give rise to completely fallacious diffusivities and, hence, inaccurately predicted concentration profiles. Here we have focussed only upon the ripple- and cycle-averaged concentration profile and its interpretation. In terms of sand transport prediction by waves or by wave+current flows this is simply the first step, since the mean concentration profile can give information about only the 'current related' component of the transport. As noted by Davies and Thorne (2005) this component may be only a relatively small part of the total transport comprising also the 'wave-related' component that depends upon intra-wave processes. They noted further how intra-ripple processes must be invoked in order to understand the mechanisms giving rise to the observation that values of β ($=\varepsilon_s/\nu_t$) are greater than unity above ripples (Section II). Davies and Thorne (2005) suggested that, in some average sense above a rippled bed, regions of high (or low) suspended concentration are correlated with regions of high (or low) vertical velocity in a way that is different from the correlation that exists between the horizontal and vertical components of velocity field. The former correlation determines the sediment diffusivity ε_s while the latter correlation determines the eddy viscosity ν_t. While these complex issues remain as key challenges for future work, the present study is believed to have elucidated a vital part of the phenomenon of sediment dynamics above ripples. The results for the sediment diffusivity ε_s presented here provide simple, critical tests for modelling systems. They also lend strong support to research modelling approaches such as presented by Davies and Thorne (2005) who used a two-layer diffusivity (including a height-constant near-bed layer) to represent quite successfully detailed sediment concentration profiles observed above steep ripples.

V1 Conclusions

Acoustic measurements have been presented of sediment diffusivity profiles above sandy rippled beds under regular, weakly asymmetrical, waves. For the two beds investigated, comprising medium and fine sand respectively, different mean suspended sediment concentration profiles were observed. For the medium sand the sediment diffusivity ε_s inferred from the concentration profiles was constant with height above the bed up to a distance of approximately $z \approx 1.3k_s$. Above this ε_s increased linearly with height. In order to explain the form of the diffusivity profile an assessment was made of the ripples on the bed and the variation of the suspended concentration with the phase of the wave. In the case of the medium sand, the steepness of the ripples indicated that flow separation on the lee-side of the ripple crest should be occurring. This was confirmed by the intra-wave suspended sediment measurements, which yielded results consistent with vortex entrainment, with the major inputs of sediment into suspension occurring around flow reversal. The formation of the vortices led to a relatively constant mixing length, resulting in a constant value for ε_s close to the bed. Above this region the vortices appeared to lose their coherence, with gradient diffusion becoming dominant, characterised by the mixing length scale growing and resulting in ε_s increasing with height above the bed. In contrast, for the fine sand, the diffusivity, ε_s, was observed to increase linearly for all heights above the bed, and no 'ε_s = constant' lower layer was present. Analysis of the ripples and the intra-wave suspended sediment showed no evidence of flow separation or vortex formation. In this case it was concluded that the bed was behaving as 'dynamically plane', with turbulent eddies growing in size with height above the bed, leading to the observed linear form for ε_s.

To compare the observed profiles of sediment diffusivity with previous empirical results, the formulations of Nielsen (1992), Van Rijn (1993) and the standard 'constant stress layer' expression were assessed. Nielsen's prediction, for very rough beds, of a constant value of ε_s in the near-bed layer, was confirmed for the medium sand and found to have a value similar to that observed, though somewhat lower. The Nielsen formulation was not applicable to the fine sand observations due to the absence of coherent near-bed mixing processes. The Van Rijn expression for ε_s captured with reasonable accuracy both the constant and also the linear diffusivity regions for the medium sand. Applying the linear component of Van Rijn's formulation to the fine sand gave a result in the outer layer that was comparable with, though an overestimate of, the observed diffusivity. Comparison of the conventional flat bed formulation, $\varepsilon_s = \beta\kappa\bar{u}_* z$, with β=1 and $k_s=25\eta_r(\eta_r/\lambda_r)$ gave substantial overestimates for the linear component of ε_s for both of the sands studied. However, if $k_s=2.5d_{50}$ was used in the evaluation of ε_s predictions were obtained which were much more comparable with the observations. It appears therefore that, in the medium sand case, where steep ripples were observed, the sediment diffusivity in the outer layer, i.e. above the vortex layer, scales approximately on the grain size associated with an equivalent flat bed. For the low slope ripples in the fine sand the sediment diffusivity behaved, both in form and also magnitude, as expected above a 'dynamically plane' bed. Based on the present observations in the Deltaflume, new empirical formulae have been proposed here for the sediment diffusivity above both steep and also low ripples that may be used in the future by other workers.

Acknowledgements

The work was supported by the European Union through its Access to Large Scale Facilities under contract MAS3-CT97-0106 and by the Natural Environment Research Council, UK. The authors would particularly like to thank Dr Jon J Williams who co-ordinated the experiment and John Humphery who was central to the deployment of the instrumentation.

References

Bell, P.S., Thorne, P.D. and Williams, J.J. 1998. Acoustic measurements of sand ripple profile evolution under controlled wave conditions. pp.353-358 in, Proceedings of the fourth European Conference on Underwater Acoustics, (eds.A.Alippi & G.B.Cannelli), Volume I. Rome: Italian National Research Council, 1003pp.

Bosman, J. 1982.Concentration measurements under oscillatory motion. Reports M1695-II and M1875, Delft Hydraulics, The Netherlands

Chung D. H. and L. C. Van Rijn. 2003 Diffusion approach for suspended sand transport under waves. J. of Coastal Research, 19, 1, 1-11.

Crawford, A.M., Hay, A.E. 1993. Determining suspended sand size and concentration from multifrequency acoustic backscatter. J. Acoust. Soc. Am. 94(6), 3312-3324.

Coleman N. L. 1970. Flume studies of sediment transfer coefficient. Water Resources Research, 6(3), 801-809.

Davies A.G., 1986. A model of oscillatory rough turbulent boundary layer flow. Estuarine, Coastal and Shelf Science, 23, 353-374.

Davies A.G. and C. Villaret, 1997. Oscillatory flow over rippled beds: Boundary layer structure and wave-induced Eulerian drift. Chapter 6 in Gravity Waves in Water of Finite Depth, ed. J.N. Hunt, Advances in Fluid Mechanics, Computational Mechanics Publications, 215-254.

DaviesA. G. and Thorne P.D. 2005. Modelling and measurement of sediment transport by waves in the vortex ripple regime. Journal of Geophysical Research. Vol 110, C05017, doi:1029/2004JC002468, 2005. pp25

Davies A.G. and P.D. Thorne 2008. Advances in the study of moving sediments and evolving seabeds. Surveys in Geophysics. In Press

Fredsøe J (1984) Turbulent boundary layer wave-current motion. J. Hydraul. Eng. 110(8):1103-1120.

Fredsoe, J. Andersen K H. Sumer, BM. 1999. Wave plus current over a ripple-covered bed . Coastal Engineering, 38, 4, 177-221.

Glenn S. M. and W. D. Grant. 1987. A suspended sediment stratification correction for combined wave and current flows. J of Geophysical Research, 92, C8, 8244-8264

Grant. W. D. and Madsen O. S. 1979. Combined wave and current interaction with a rough bottom. J of Geophysical Research, 84, C4, 1797-1808.

Hansen E. A., Fredsoe J. And Deigard R. 1991. Distribution of suspended sediment over wave generated ripples. International Symposium on The transport of suspended sediments and its mathematical modeling. Held in Florence, Italy, September 2-5 1991.111-127

Lee T. H. and Hanes D. M. 1996. Comparison of field observations of the vertical distribution of suspended sand and its prediction by models. J. Geophysical Research 101,C2,3561-3572.

Lee G, Friedrichs C. T and Vincent C.E. 2002. Examination of diffusion versus advection dominated sediment suspension on the inner shelf under storm and swell conditions, Duck, North Carolina. J. Geophysical Research 107, C7, 3084, 10.1029/2001JC000918. 21.1-21.13.

Magar V. and Davies A.G., 2005. Suspended sediment dynamics over rippled beds in oscillatory flows based on a 2DHV discrete-vortex / particle-tracking model. Pp. AG 1-9 in SANDPIT, Sand Transport and Morphology of Offshore Mining Pits, by L.C. Van Rijn, R.L. Soulsby, P. Hoekstra and A.G. Davies (Eds.), Aqua Publications, The Netherlands.

Nielsen P. 1986. Suspended sediment concentration under waves. Coastal Engineering, 10, 23-31.

Nielsen P. 1988. Three simple models of wave sediment transport. Coastal Engineering, 12, 43-62.

Nielsen P. (1992). Coastal Bottom Boundary Layers and Sediment Transport. Advanced series on ocean engineering, volume 4. World Scientific, Singapore, 324 pp.

Nielsen P and Teakle A. L. 2004. Turbulent diffusion of momentum and suspended particles: A finite-mixing-length theory. Physics of Fluids, 16, 7, 2342-2348.

Nowell A. R. M. and C. E. Long. 1983. An evaluation of von Karmen's constant. In: Hickley, B. M. (Editor) Pollutant transfer and sediment dispersal in the Washingto-Oregon coastal zone: Report of progress, 1 August 1982- 31 July 1983, Department of energy, University of Washington, Report RLO 2225 TA25-64.

Nezu I and Rodi W. 1986. Open-channel flow measurements with a laser Doppler anemometer. J of Hydraulic Engineering, 112, 5, 335-355.

O'Donoghue, T., Doucette, J. S, Van der Werf J. J. and Ribberink J. S. 2006. The dimensions of sand ripples in full-scale oscillatory flows. Coastal Engineering 53, 997-1012 .

Ogston A. S. and Sternberg R. W. 2002. Effect of wave breaking on sediment eddy diffusivity, suspended sediments and longshore sediment flux profiles in the surf zone. Continental Shelf Research, 22, 4, 633-655.

Osborne P D. and Vincent C. E. 1996. Vertical and horizontal structure in suspended sand concentrations and wave induced fluxes over bedforms. Marine Geology, 131,195-208.

Ranasoma, K.I.M., and . Sleath J. F. A. 1992. Velocity measurements close to rippled beds, in Proceedings of the 23rd International Conference on Coastal Engineering, pp. 2383-2396, American Society of Civil Engineers, Venice, Italy.

Ribberink J. S. and Al-Salem A. A. 1994. Sediment transport in oscillatory boundary layers in cases of rippled beds and sheet flow. J. of Geophysical Research, 99, C6, 12707-12727.

Rose C. P. and Thorne P. D.. 2001. Measurements of suspended sediment transport parameters in a tidal estuary. Continental and Shelf Research, 21, 1551-1575.

Sheng J and Hay A. E. 1995. Sediment eddy diffusivities in the nearshore zone, from multifrequency acoustic backscatter. Continental Shelf Research, 15, 2/3, 129-147.

Sleath J. F. A. 1982. The suspension of sand by waves. J. of Hydraulic Research, 20, 5, 439-452.

Sleath J F A. 1984 Sea Bed Mechanics. John Wiley publications USA. 335 pp.

Sleath, J.F.A., Velocities and shear stresses in wave-current flows. 1991. J. Geophysical Research, 96, C8, 15,237-15,244.

Soulsby R. L. 1997 Dynamics of marine sands. Thomas Telford publication, UK. 249 pp.

Swart, D.H., 1974. “Offshore sediment transport and equilibrium beach pro-files.” Publ. 131, Delft Hydrol. Lab., Delft, Netherlands.

Thorne, P.D., Hardcastle, P.J., Soulsby, R.L., 1993. Analysis of acoustic measurements of suspended sediments, J. of Geophysical Res., Vol. 98, No. C1, 899-910.

Thorne, P. D. Williams, J. J. AND Davies, A. G. 2002. Suspended sediments under waves measured in a large scale flume facility. J. Geophysical Research. Vol 107, No C8, 4.1-4.16

Thorne, P. D. and Hanes D. M. 2002. A review of the application of acoustics to small scale sediment processes. Continental Shelf Research, 22, 4, 603-632.

Thorne P. D., Davies A. G. and Williams J.J. (2003). Measurements of near-bed intra-wave sediment entrainment above vortex ripples. Geophysical Research Letter, 30, 20, 2028. 2.1-2.4. doi:1029/2003GL018427.

Trowbridge J.H. and Madsen O. S. 1984. Turbulent wave boundary layers. 1. Model formulation and first order solution. Journal of Geophysical Research, 89, C5, 7989-7997.

van der Werf J. J. Ribberink, J. S, O'Donoghue T and Doucette J. S. 2006. Modelling and measurement of sand transport processes over full-scale ripples in oscillatory flow. Coastal Engineering, 53, 657-673

van der Werf J. J, Doucette J. S, O' Donoghue T and Robberink J. S. 2007. Detailed measurements of velocities and suspended sediments over full-scale ripples in regular oscillatory flow. Journal of Geophysical Research, 112, F02012, doi:10.1029/2006JF000614.

Van Rijn L. C. 1984. Sediment transport part II. J of Hydraulic Engineering, 110, 11, 1613-1641.

Van Rijn L. C., 1993 Principles of sediment transport in rivers, estuaries and coastal seas. Aqua publications, the Netherlands. 633 pp.

Van Rijn L. C., Davies, A. G, Van de Graff J and Ribberink J. S. 2001 Sediment transport and modeling in marine coastal environments. Aqua publications, the Netherlands. 415 pp.

Villard P. V. and Osborne. P. D. 2002. Visualisation of wave-induced suspension patterns over two-dimensional bedforms. Sedimentology, 49, 363-378

Vincent C E, and Green M. O. 1990. Field measurements of the suspended sand concentrations and fluxes and of the resuspension coefficient γ_o over a rippled bed. J. Geophysical Research, 95, C7, 11591-11601.

Vincent C. E. and Osborne P. D. 1995. Predicting suspended sand concentration profiles on a macro-tidal beach. Continental Shelf Research, 15, 13, 1497-1514.

Vincent C. E, Marsh S. W, Webb M. P and Osborne P. D. 1999. Spatial and temporal structures of suspensions and transport over megaripples on the shore face. J. Geophysical Research, 104, C5, 11215-11224.

Whitehouse R. 1995. Observations of the boundary layer characteristics and the suspension of sand at a tidal site. Continental Shelf Research., 15, 13, 1549-1567.

Williams J. J, Bell P S, Coates L E, Metje N and Selwyn R. 2003. Interactions between a benthic tripod and waves on a sandy bed. Continental Shelf Research, 23, 355-375.

Williams J.J., Bell .P S, Thorne P. D., Metje N and Coates L E. 2004. Measurements and prediction of wave-generated suborbital ripples. Journal of Geophysical Research. Vol 109 CO2004. doi:10.1029/2003JC001882. pp1-18

Tables

Bed form characteristics	**2D Steep Ripples**	**2D and 3D Transitional Ripples**	**Dynamically Plane Bed**
Ripple steepness η_r/λ_r	$\eta_r/\lambda_r \geq 0.12$	$0.08 \leq \eta_r/\lambda_r \leq 0.12$	$\eta_r/\lambda_r \leq 0.08$
Relative roughness A_0/k_s	O(1)	O(1-10)	O(100-1000)
Reynolds number RE	$O(10^3\text{-}10^4)$	$O(10^4\text{-}10^5)$	$O(10^6\text{-}10^7)$
Peak Shields Parameter $\hat{\theta}$	$0.05 \leq \hat{\theta} \leq 0.2$	$0.2 \leq \hat{\theta} \leq 0.7$	$\hat{\theta} \geq 0.7$

Table 1. Bed form characteristics related approximately to boundary layer flow characteristics.

Figure Captions

Fig 1 Schematic of the instrumented tripod used for the measurements; STABLE- **S**ediment **T**ransport **A**nd **B**oundary **L**ayer **E**quipment. Shown is the triple frequency acoustic back scatter system, ABS, operating at 1 MHz, 2 MHz, and 4MHz, the acoustic ripple (bed) profiler, ARP, the pumped sampling heights and the electromagnetic current meters, ECMs.

Fig2. Measurements of burst averaged concentration profiles at the three frequencies for fine (×,*,Δ) and medium (o,+,□) sands for a) H=0.5 m and b) H=0.8 m, both had periods of 5s.

Fig 3. All the measurements of the sediment diffusivity with height above the undisturbed bed level for the medium sand.

Fig 4 Measurements of the normalised sediment diffusivity (·), with three estimates of the mean; o filtered, Δ median , + trimmed, with normalised height above the medium sand bed.

Fig 5. Comparison of the mean measured normalised sediment diffusivity (●) over the medium sand bed, with the calculations from equations (8) (····), (9-11) (----), (17) (x,+, see text) and (18) (─).

Fig 6. a) Measurements for the medium sand bed of; a) a transect of the bed over time for an experimental run with H=0.81 m and T= 5s , b) the ripple slopes and c) the equivalent bed roughness for all experimental runs.

Fig 7. Measurement of the variation in concentration with the phase of the wave and height above the bed for the medium sand. a) The wave velocity at 0.31 m above the bed and b) the suspended sediment concentration. The wave conditions were H=1.06 m and T=5s.

Fig 8. All the measurements of the sediment diffusivity with height above the undisturbed bed level for the fine sand.

Fig 9. Measurements of the normalised sediment diffusivity (·), with three estimates of the mean; o filtered, Δ median , + trimmed with normalised height above the fine sand bed.

Fig 10. Comparison of the measured normalised sediment diffusivity (●) over the fine bed, with the predictions from equations (19) (– –), (17) (x,+ see text) and (20) (—)

Fig 11. a) Measurements for the fine sand bed of; a) a transect of the bed over time for an experimental run with H=0.79 m T=5s, b) the ripple slopes and c) the equivalent bed roughness for all experimental runs.

Fig 12. Measurement of the variation in concentration with the phase of the wave and height above the fine bed. a) The wave velocity at 0.31 m above the bed and b) the suspended sediment concentration. The wave conditions were H=0.82 m and T=5s.

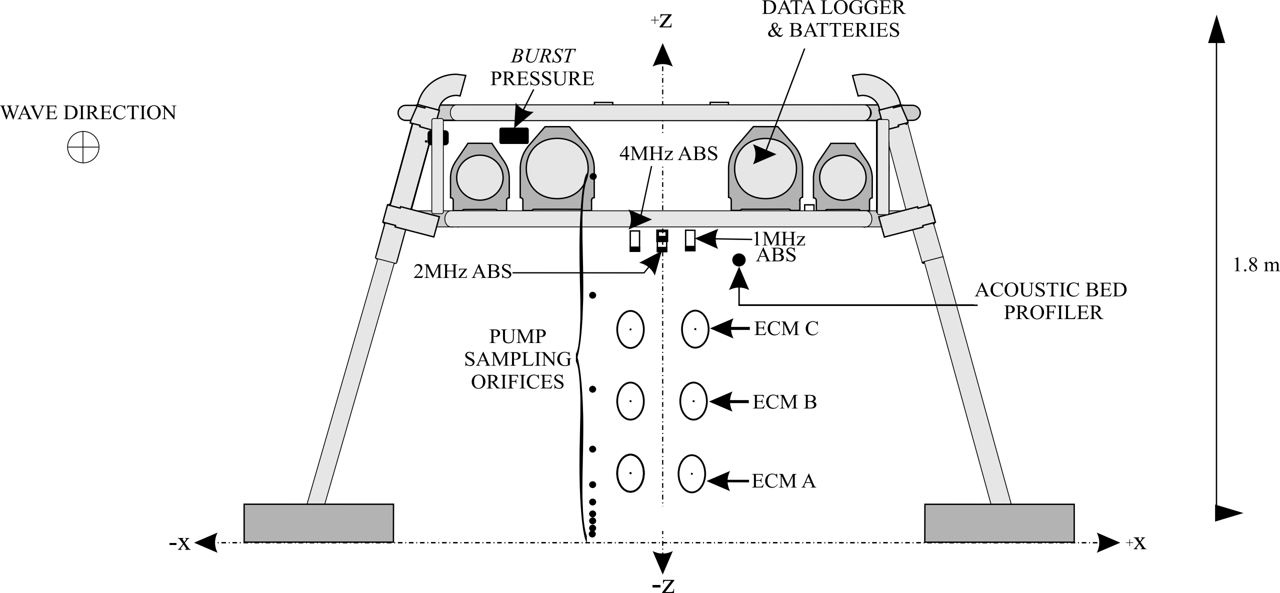

+Z
DATA LOGGER
& BATTERIES
BURST
PRESSURE
WAVE DIRECTION
4MHz ABS
1MHz
ABS
2MHz ABS
1.8 m
ACOUSTIC BED
PROFILER
ECM C
PUMP
SAMPLING
ORIFICES
ECM B
ECM A
-x
+x
-Z

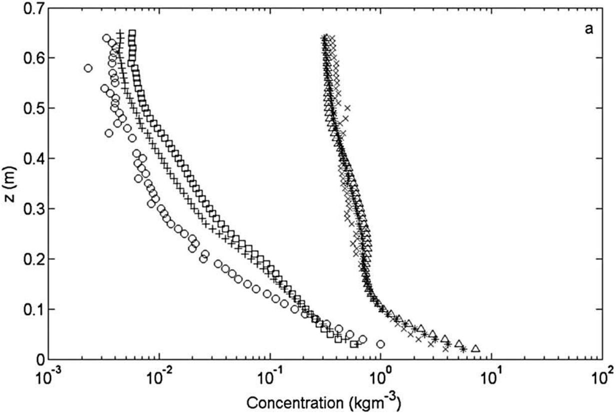
a
z (m)
Concentration (kgm^{-3})
0.7
0.6
0.5
0.4
0.3
0.2
0.1
0
10^{-3}
10^{-2}
10^{-1}
10^{0}
10^{1}
10^{2}

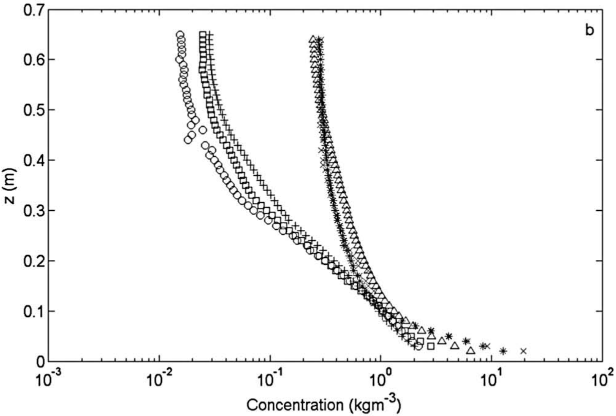
b
z (m)
Concentration (kgm^{-3})
0.7
0.6
0.5
0.4
0.3
0.2
0.1
0
10^{-3}
10^{-2}
10^{-1}
10^{0}
10^{1}
10^{2}

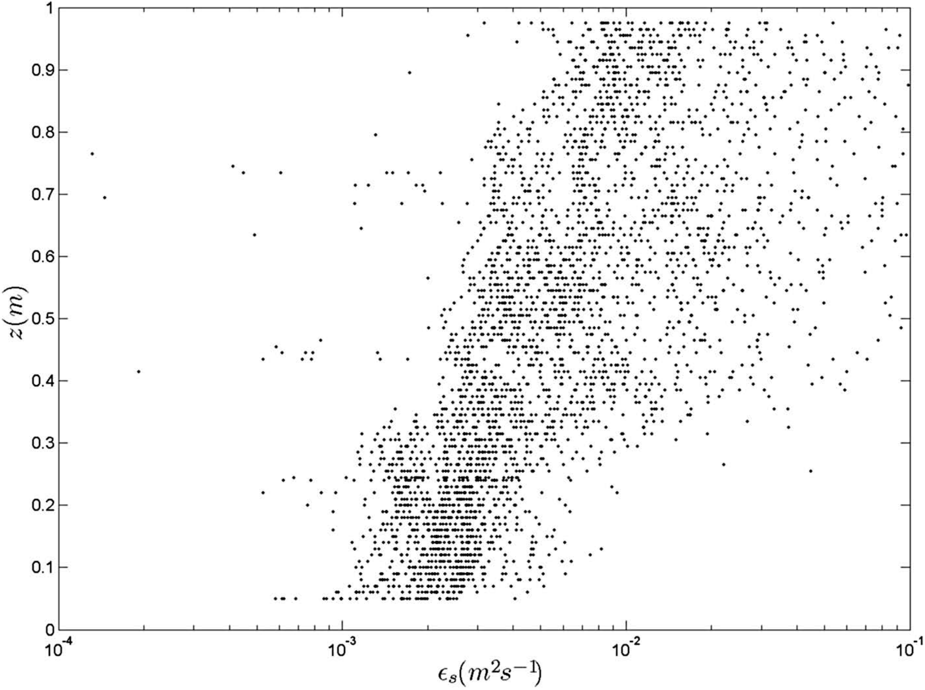
1
0.9
0.8
0.7
0.6
0.5
0.4
0.3
0.2
0.1
0
$z(m)$
10^{-4}
10^{-3}
10^{-2}
10^{-1}
$\epsilon_s(m^2s^{-1})$

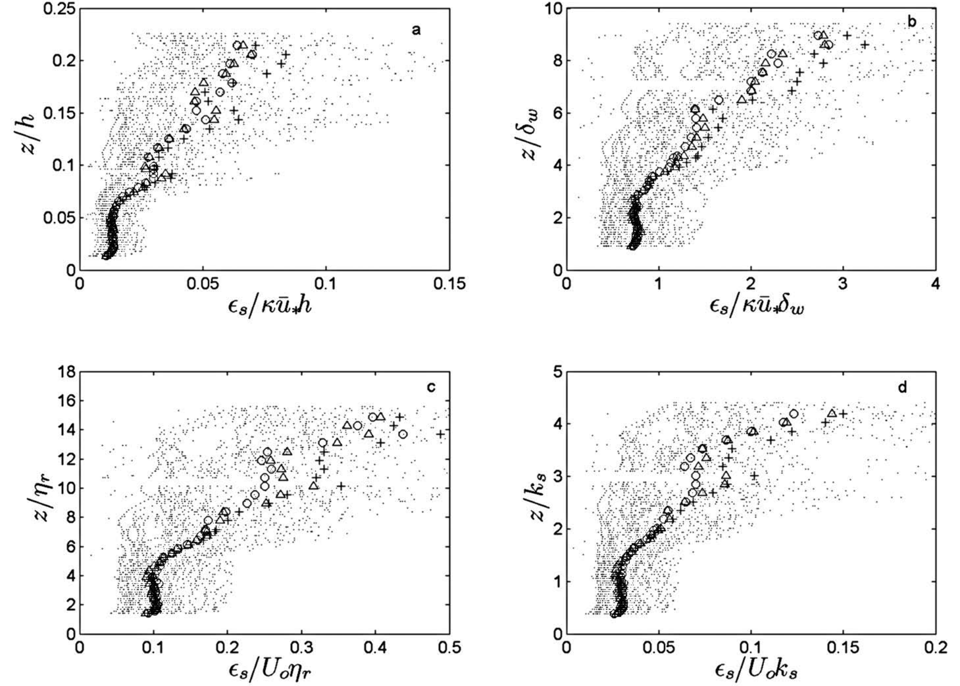
a
b
c
d
z/h
$\epsilon_s/\kappa\bar{u}_* h$
z/δ_w
$\epsilon_s/\kappa\bar{u}_* \delta_w$
z/η_r
$\epsilon_s/U_o\eta_r$
z/k_s
$\epsilon_s/U_o k_s$

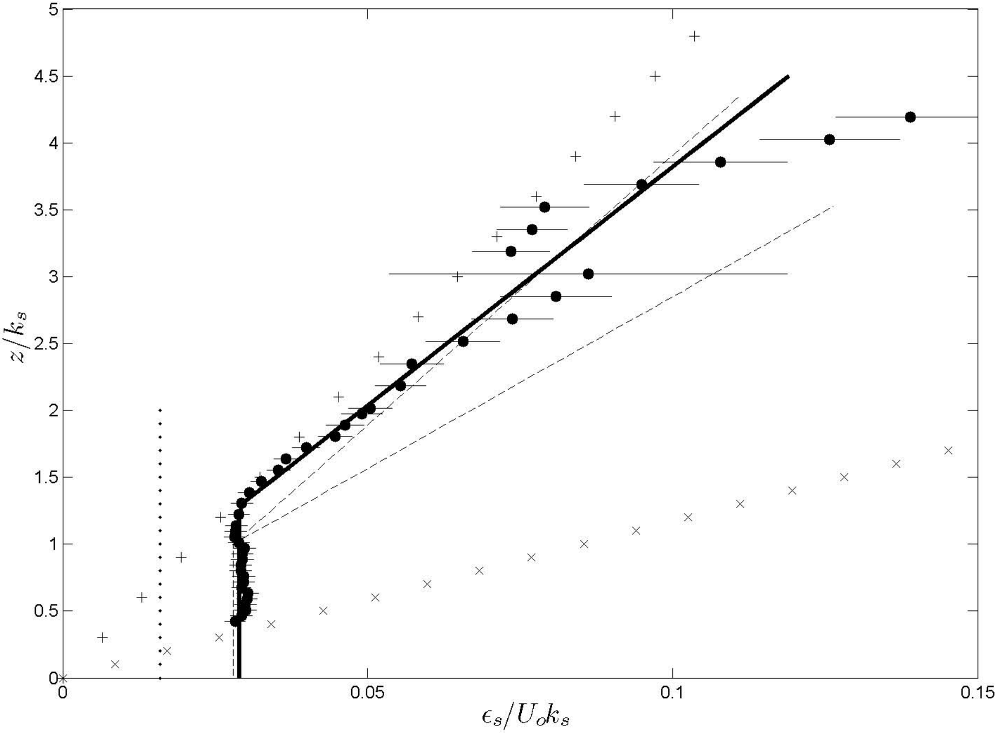

5
4.5
4
3.5
3
2.5
2
1.5
1
0.5
0
z/k_s
0
0.05
0.1
0.15
$\epsilon_s/U_o k_s$

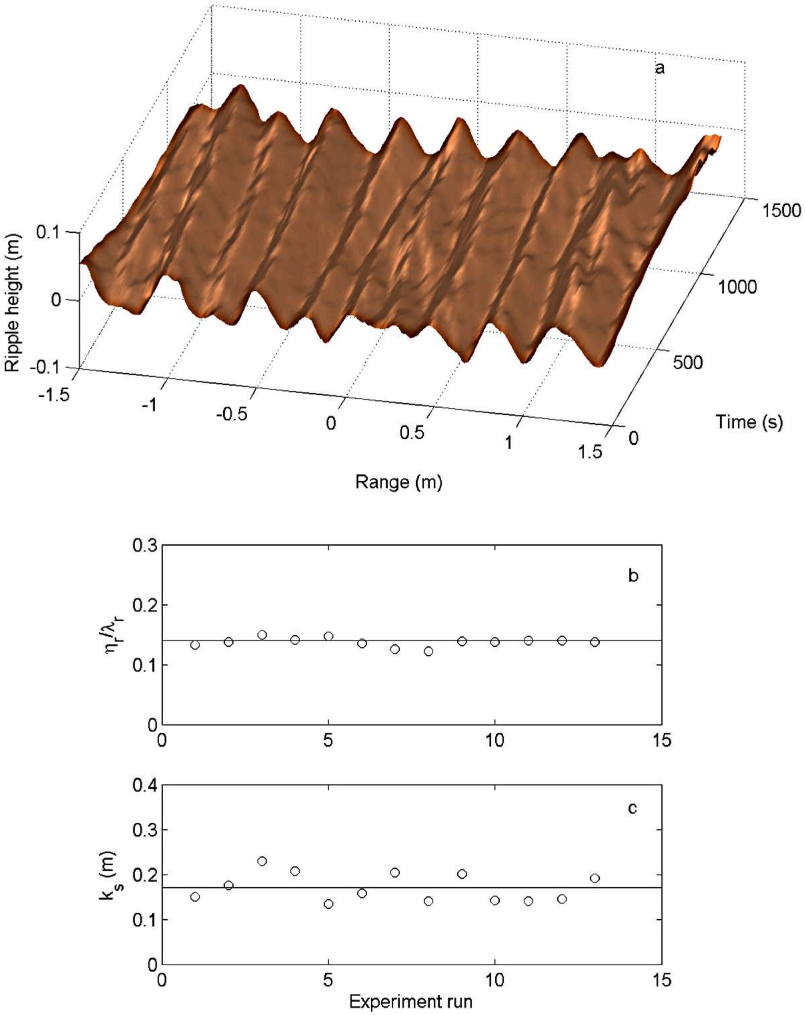
a
Ripple height (m)
0.1
0
-0.1
-1.5
-1
-0.5
0
0.5
1
1.5
Range (m)
0
500
1000
1500
Time (s)
b
η_r/λ_r
0.3
0.2
0.1
0
0
5
10
15
c
k_s (m)
0.4
0.3
0.2
0.1
0
0
5
10
15
Experiment run

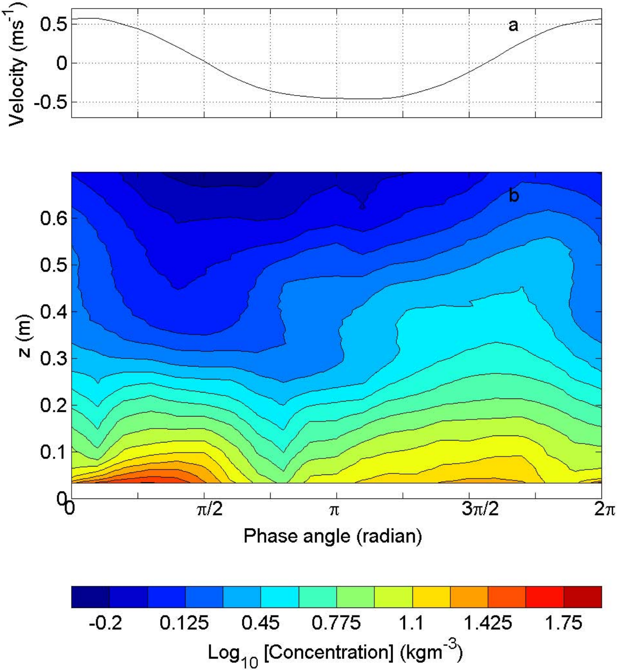
Velocity (ms-1)
0.5
0
-0.5
a
b
z (m)
0.6
0.5
0.4
0.3
0.2
0.1
0
0
π/2
π
3π/2
2π
Phase angle (radian)
-0.2
0.125
0.45
0.775
1.1
1.425
1.75
Log10 [Concentration] (kgm-3)

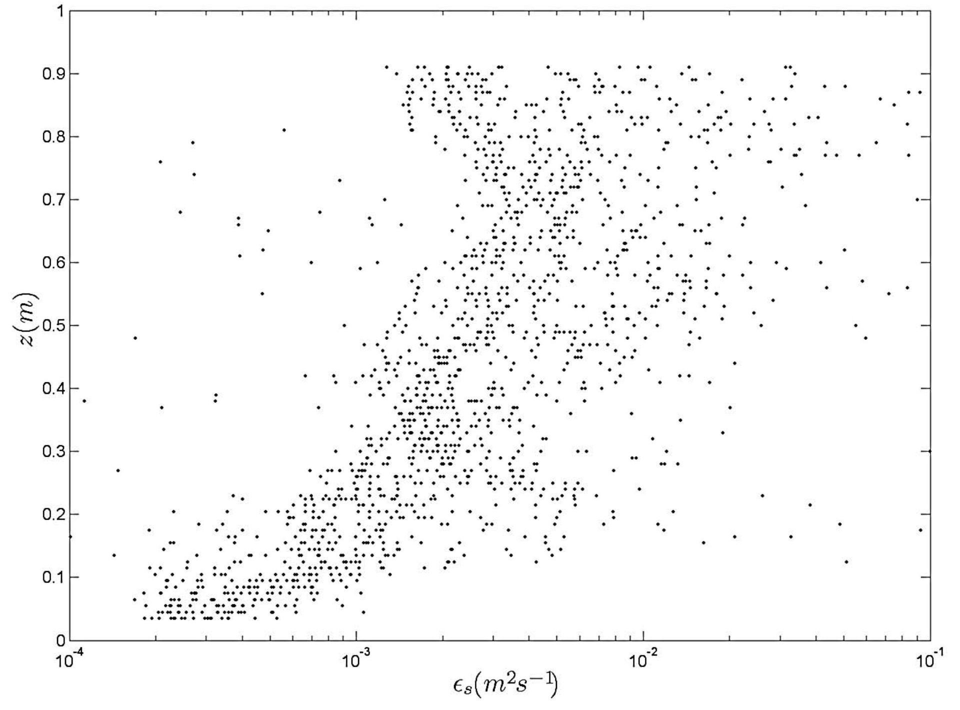

1
0.9
0.8
0.7
0.6
0.5
0.4
0.3
0.2
0.1
0
$z(m)$
10^{-4}
10^{-3}
10^{-2}
10^{-1}
$\epsilon_s(m^2s^{-1})$

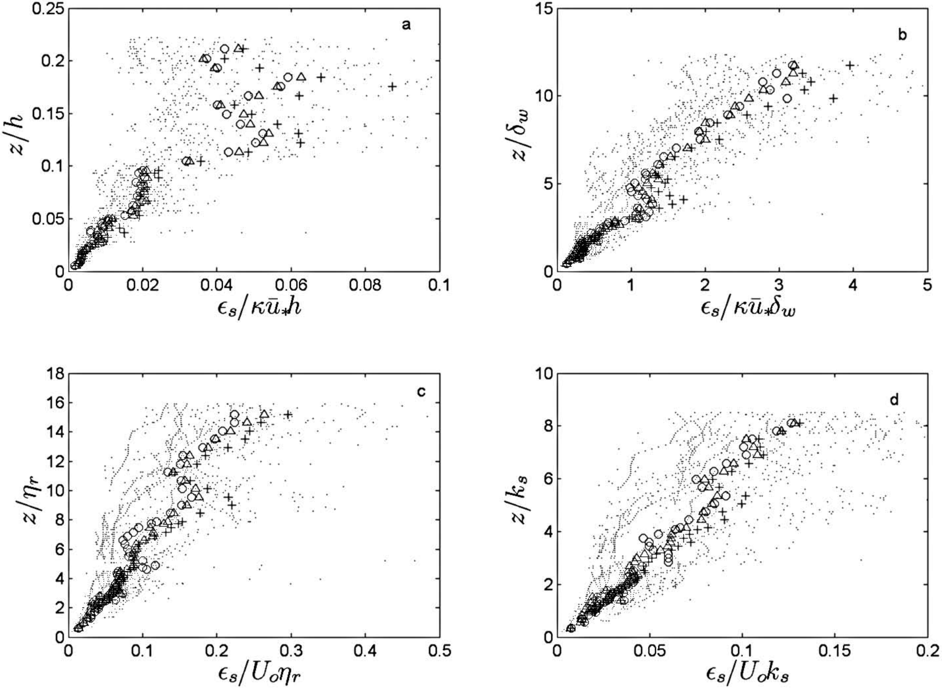

a
b
c
d
z/h
$\epsilon_s/\kappa\bar{u}_*h$
z/δ_w
$\epsilon_s/\kappa\bar{u}_*\delta_w$
z/η_r
$\epsilon_s/U_o\eta_r$
z/k_s
ϵ_s/U_ok_s

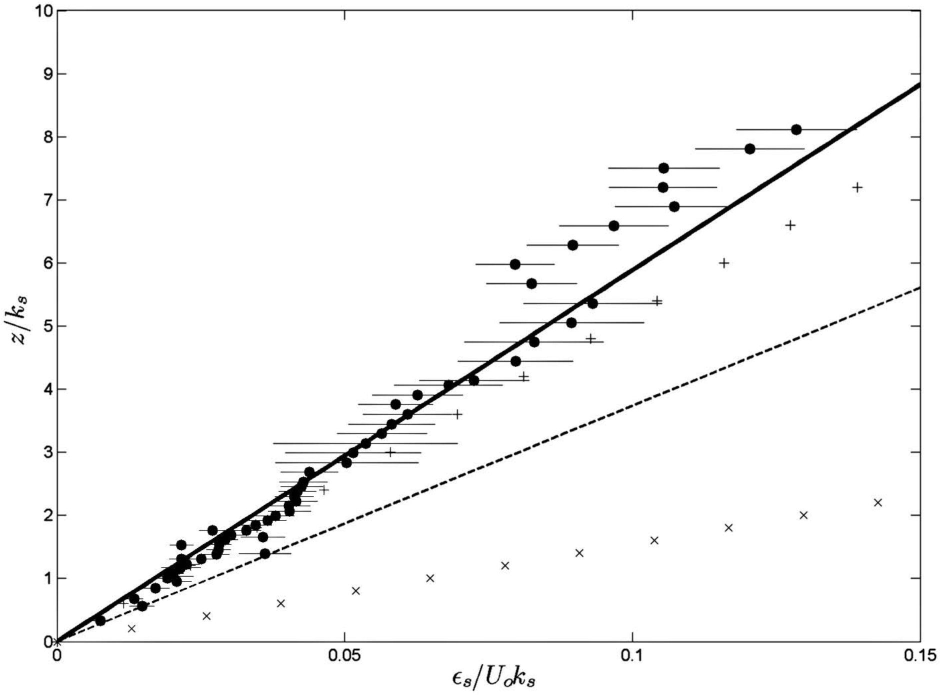

10
9
8
7
6
5
4
3
2
1
0
0
0.05
0.1
0.15
z/k_s
$\epsilon_s/U_o k_s$

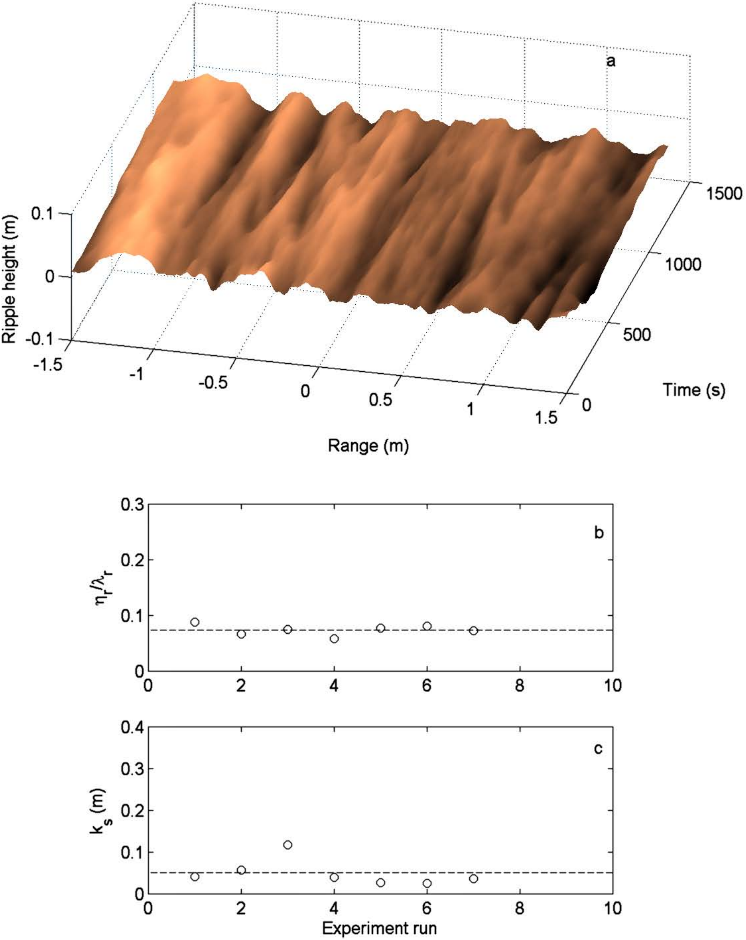
a
Ripple height (m)
0.1
0
-0.1
-1.5
-1
-0.5
0
0.5
1
1.5
Range (m)
0
500
1000
1500
Time (s)
b
η_r/λ_r
0.3
0.2
0.1
0
0
2
4
6
8
10
c
k_s (m)
0.4
0.3
0.2
0.1
0
0
2
4
6
8
10
Experiment run

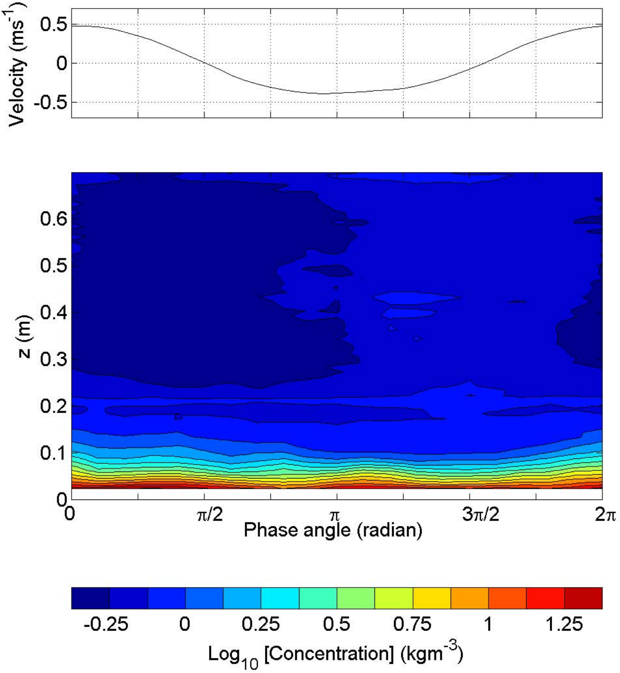

Velocity (ms^-1)
0.5
0
-0.5
z (m)
0.6
0.5
0.4
0.3
0.2
0.1
0
π/2
π
3π/2
2π
Phase angle (radian)
-0.25
0
0.25
0.5
0.75
1
1.25
Log10 [Concentration] (kgm^-3)